Bond Angle Distributions of Carbon Dioxide in the Gas, Supercritical, and Solid Phases[†]

Kelly E. Anderson, Steven L. Mielke, J. Ilja Siepmann,* and Donald G. Truhlar*

Department of Chemistry and Minnesota Supercomputing Institute, University of Minnesota, 207 Pleasant St. SE, Minneapolis, Minnesota 55455-0431

Received: October 1, 2008; Revised Manuscript Received: December 10, 2008

Recent work has focused attention on possible shifts in the bond angle distribution of CO_2 as a consequence of intermolecular interactions in the supercritical phase. To investigate the temperature and phase dependence of the intramolecular structure of CO_2, we performed Feynman path integral Monte Carlo calculations based on a spectroscopically derived analytical potential, first principles molecular dynamics simulations using Kohn−Sham density functional theory, and Monte Carlo simulations employing empirical interaction potentials. On the basis of various distributions used to characterize the intramolecular structure, we conclude that the aggregation state has a negligible influence on the intramolecular structure, in particular we find that in the classical limit the distributions are remarkably similar for the ideal gas, supercritical, and solid phases when considered at the same temperature. In contrast, an increase in the temperature from 325 to 673 K or inclusion of nuclear quantum effects leads to a significant broadening of the distributions. With respect to the first C−O bond vector, the second bond vector most prefers a collinear arrangement. However, due to the Jacobian factor the maximum in the bond angle distribution at 325 K is shifted to an angle of about 175.7° in the classical limit or to 173.0° if nuclear quantum effects are included. Nevertheless, an analysis of the temperature dependence of the constant-volume heat capacity demonstrates that carbon dioxide should be viewed as a linear molecule.

1. Introduction

Supercritical fluids are attractive solvents for a variety of applications because they combine to some extent the positive attributes of gaseous and liquid phases, and their properties can be tuned easily by changing the temperature or pressure or by addition of cosolvents.[1−9] Many common applications exploit this property, including supercritical fluid extraction and chromatography. Carbon dioxide (CO_2) is a particularly useful supercritical solvent as it is nontoxic and nonflammable and has a readily accessible critical point (T_{crit} = 304.3 K, p_{crit} = 73.8 bar).

Given the technological interest in supercritical CO_2 ($scCO_2$) as a green solvent, it is not surprising that its thermodynamic, structural, and transport properties have been the subject of many experimental and computational investigations. Motivated by some recent computational studies,[10−13] we focus in this work on the intramolecular structure of CO_2. From an analysis of the trajectory of a Car−Parrinello molecular dynamics simulation of $scCO_2$, Saharay and Balasubramanian found a maximum at 174.2° for the distribution of the bond angle and argued that "the nonlinearity in the O−C−O angle in $scCO_2$ is a consequence of the formation of a first neighbor shell".[11] The distribution shown in their paper corresponds to a distribution of the instantaneous average of all the bond angles computed for a 32-molecule system.[11] In a subsequent paper by the same authors, the cosine distributions of individual O−C−O angles obtained from Car−Parrinello molecular dynamics simulations of $scCO_2$ at different densities are compared to those obtained from molecular dynamics simulations for a semirigid empirical model,[13] and it is surmised that the differences are "due to polarization effects induced by a changing near-neighbor environment".[12]

Inspired by this apparent nonlinearity of $scCO_2$, Zhang et al.[13] proposed modifications of the empirical rigid linear CO_2 model of Harris and Yung,[14] to introduce rigid and semirigid models with an equilibrium bond bending angle of 174.2° (which, together with the use of partial charges, leads to the introduction of a spurious permanent dipole). Recently, the resulting rigid bent EPM-M model was used to analyze the data of neutron diffraction experiments for supercritical mixtures of CO_2 and water.[15,16] However, this view of the intramolecular structure of $scCO_2$ is in conflict with neutron diffraction experiments[17,18] for CO_2 in the gaseous, liquid, and supercritical states that generally show $2r_{CO} \cong r_{OO'}$ and that led Ishii et al. to conclude "that the intramolecular C−O and O−O distances are independent of the conditions and that the carbon dioxide molecule is linear-shaped".[18] We note that values of 0.9990 and 0.9995 for the ratio of $r_{OO'}/2r_{CO}$ correspond to bend angles of 174.9° and 176.4°, respectively. Thus, diffraction experiments would need to determine the intranuclear distances with a precision of at least 4 significant figures to support the argument that the bend angle is larger than 175°. Indeed, some fits to experimental diffraction data[18,19] yield $r_{OO'} > 2r_{CO}$, i.e., an impossible set of internuclear distances. Somewhat in contrast to the more recent neutron diffraction studies, an earlier study found internuclear distances that support a bend angle of 163° for liquid CO_2.[20]

In this work, we use several computational techniques, including path integral Monte Carlo calculations, first principles molecular dynamics simulations, and Monte Carlo simulations for empirical models, to investigate the intramolecular structure of CO_2 for various aggregation states and temperatures. Furthermore, we compute the constant-volume heat capacity because the change from a linear geometry to a nonlinear geometry results in replacing one vibrational degree of freedom

[†] Part of the "Max Wolfsberg Festschrift".

* Corresponding authors. E-mail: siepmann@umn.edu and truhlar@umn.edu.

10.1021/jp808711y CCC: $40.75
Published on Web 01/27/2009

TABLE 1: Mean Internuclear Distances, Internuclear Distance Ratios, Bend Angles, and Cosines of the Bend Angle for CO_2[a]

temp [K]	method	$\langle r_{CO}\rangle$ [Å]	$\langle r_{OO}\rangle$ [Å]	$\langle r_{OO}/r_{CO} + r_{CO}\rangle$	$\langle\theta\rangle$ [deg]	$\langle\cos\theta\rangle$
325	PIMC ($P = 256$)	1.165_{35}	2.325_{40}	0.9976_{23}	173.0_{36}	-0.9906_{94}
	PIMC ($P = 1$)	1.162_{17}	2.320_{23}	0.9986_{14}	174.6_{28}	-0.9943_{57}
	FPMD (solid)	1.170_{18}	2.336_{23}	0.9984_{16}	174.3_{30}	-0.9937_{65}
	FPMD (scf-low[b])	1.180_{18}	2.356_{24}	0.9985_{15}	174.5_{29}	-0.9941_{59}
	FPMD (scf-high[c])	1.176_{18}	2.348_{23}	0.9985_{15}	174.3_{29}	-0.9938_{60}
	semirigid		2.317_{3}	0.9986_{14}	174.6_{28}	-0.9943_{57}
673	PIMC ($P = 128$)	1.166_{36}	2.324_{43}	0.9965_{34}	171.5_{44}	-0.9862_{136}
	PIMC ($P = 1$)	1.164_{25}	2.321_{34}	0.9970_{29}	172.2_{41}	-0.9882_{117}
	FPMD (scf-high)	1.178_{26}	2.349_{34}	0.9970_{31}	172.2_{42}	-0.9882_{122}
	semirigid		2.313_{7}	0.9971_{29}	172.2_{41}	-0.9883_{117}

[a] Subscripts denote the root-mean-square deviations of the final two or three digits of the mean. The standard errors of the mean are less than ±1 in the last digit quoted for the PIMC calculations and the MC simulations for the semirigid model, and less than ±3 in the last digit quoted for the FPMD simulations. [b] Specific density of 0.80 g/cm^3. [c] Specific density of 1.88 g/cm^3.

TABLE 2: Rovibrational Contributions to the Heat Capacity in Units of *R*

method	325 K	673 K	1100 K	2000 K
EOS[a]	2.114	3.393	4.163	
PIMC[b] ($P = 1$)	5.017_{10}	5.029_{9}	5.046_{6}	5.114_{3}
PIMC[b] (extrapolated to $P = \infty$)	2.117_{14}	3.395_{6}	4.178_{5}	4.778_{7}
classical RR/HO: linear	5.000	5.000	5.000	5.000
RR/HO: linear, fundamental	2.037	3.365	4.124	4.675
RR/HO: linear, harmonic	2.095	3.366	4.118	4.671
classical RR/HO: bent	4.500	4.500	4.500	4.500
RR/HO: bent, fundamental	2.091	3.018	3.685	4.194
RR/HO: bent, harmonic	2.094	3.022	3.681	4.191

[a] These values are obtained by subtracting 1.5 *R* and the excess heat capacity at $p = 0.1$ MPa from the corresponding EOS value.[45] [b] The subscripts denote uncertainties given as symmetric 95% confidence intervals in the last digit(s) for the PIMC calculations.

with one rotational degree of freedom (in the rigid-rotor/harmonic-oscillator approximation[21]), which leads to significant changes in the heat capacity.

2. Computational Methods

A. Path Integral Monte Carlo Calculations. Feynman path integral Monte Carlo (PIMC) calculations[22,23] were performed to obtain properties for an isolated CO_2 molecule using one of the potentials of Chedin;[24] specifically using the parameters given in the second column of Table 2 of his paper, together with a value for the equilibrium C−O separation of 1.160 Å (for which no recommended value was supplied). This potential predicts low energies for some physically unimportant regions where the energy should be very large and this can be problematic for Monte Carlo sampling methods. To prevent such complications we replaced the evaluated energy with a large value for any configuration having $r_{CO} > 2.70\ a_0$.

The partition functions, coordinate probability distributions, and averages were calculated using a discretized Feynman path integral method employing a *P*-point trapezoidal Trotter approximation of the paths. Most of the numerical details of our implementation have been presented previously and need not be reiterated here.[25−28]

Additionally, we calculate rotational−vibrational heat capacities, $C^{\mathrm{rovib}}(T)$, directly from the internal partition function via the expression

$$C^{\mathrm{rovib}}(T) = R\beta^2 \frac{\partial^2 \ln Q}{\partial \beta^2} = 2RT \frac{\partial \ln Q}{\partial T} + RT^2 \frac{\partial^2 \ln Q}{\partial T^2} \quad (1)$$

where the derivatives are evaluated by 3-point finite difference formulas, $\beta = 1/k_B T$ with *T* the absolute temperature and k_B the Boltzmann constant, *R* is the molar gas constant, and *Q* is the partition function. Heat capacities obtained using eq 1 are not especially sensitive to the choice of step size whereas we have observed that similar formulas such as

$$C^{\mathrm{rovib}}(T) = R\left[\frac{\beta^2}{Q}\frac{\partial^2 Q}{\partial \beta^2} - \left(\frac{\beta}{Q}\frac{\partial Q}{\partial \beta}\right)^2\right] \quad (2)$$

which involve the partition function rather than the logarithm of the partition function display a strong sensitivity to the step size and sometimes need to be evaluated using higher order finite difference approximations. A crucial feature of evaluating heat capacities via finite differences[29,30] is that the samples used for calculating the partition functions need to be strongly correlated; otherwise, statistical uncertainties would lead to finite difference errors in the temperature derivatives. In the method we employ here, every path included in a calculation at a temperature *T* is also present in a calculation at *T′* except that they are scaled by a factor of $(\beta'/\beta)^{1/2}$; this approach is equivalent to a recommendation by Yamamoto.[30] When calculated in this manner, the error from the finite difference approximation has only an extremely weak dependence on the sampling, so estimates for appropriate step sizes may be made using calculations with a small number of samples; for our final calculations we selected step sizes of 0.5, 0.5, 1.0, or 8.0 K near $T = 325$, 673, 1100, and 2000 K, respectively.

The heat capacity displays slow convergence with respect to the path discretization size, *P*, and the partition function converges only slightly more rapidly with *P*. For $T = 325$ K, a value of $P = 256$ was chosen, and $P = 128$ was chosen at higher temperatures. At the lowest temperature, data were also simultaneously collected for $P = 64$ and 128, using the enhanced same path (ESP) scheme;[28] these additional data are obtained for virtually no additional expense as a byproduct of the $P = 256$ calculation. An extrapolation correction[26−28] was applied to obtain the converged quantum mechanical (QM) partition functions using the result of a fit to

$$Q^{[P]}(T) = Q^{[P=\infty]}(T) + \frac{A(T)}{P^2} + \frac{B(T)}{P^3} \quad (3)$$

Although the magnitudes of the extrapolation corrections are only about 0.05% for the calculations presented here, attempts to obtain heat capacity values directly from finite difference calculations on extrapolated partition functions still led to very large errors so heat capacities were extrapolated by applying an analogue of eq 3 directly to C^{rovib}.

The distributions of various coordinates and their average values converge much more rapidly with respect to *P* than the partition functions and heat capacities so these data need no extrapolation corrections.

Calculations for $P = 1$, which yield classical anharmonic partition functions, were also performed and need to be calculated separately from other values of P. Calculations for all P were performed at four temperatures: 325, 673, 1100, and 2000 K. At each temperature several (3 to 6) independent calculations were run with 10^7 to 10^9 Monte Carlo samples to obtain statistical uncertainties.

B. First Principles Molecular Dynamics Simulations. First principles molecular dynamics (FPMD) simulations were performed using the CP2K simulation package,[31] which uses an implementation of the Gaussian plane wave (GPW) method[32] to calculate forces and energies. On the basis of the Kohn−Sham formulation of density functional theory,[33] the GPW method uses atom-centered Gaussian basis sets to expand the Kohn−Sham orbitals and plane wave auxiliary basis sets to expand the electronic density. For these studies, the BLYP functional[34,35] was used in conjuction with a Gaussian triple-ζ valence basis set augmented with two sets of polarization functions[36] and the pseudopotentials of Goedecker, Teter, and Hutter[37] with a charge density cutoff of 280 Ry.

All FPMD simulations were performed in the canonical ensemble. Four state points were examined: three fluid phases at $\rho = 0.80$ g/cm^3 (low density) and $T = 325$ K and $\rho = 1.88$ g/cm^3 (high density) and $T = 325$ and 673 K and $N = 12$ molecules, and one solid phase at 325 K and $\rho = 2.17$ g/cm^3 ($N = 32$ molecules). The initial structures for the fluid phases were taken from simulations using an empirical potential, while the solid phase was constructed by replicating the experimental unit cell ($2 \times 2 \times 2$). A geometry optimization was performed on each starting structure using CP2K, followed by at least 20 ps of simulation with a time step of 1 fs. All ensemble properties are averaged over the final 15 ps of the CP2K trajectory. Massive Nosé−Hoover chain (NHC) thermostats (i.e., one NHC per atom) were used to regulate the temperature.[38]

C. Monte Carlo Simulations Using Empirical Force Fields. Carbon dioxide was represented as a three-site model with the interaction sites located at the positions of the carbon and oxygen nuclei. Intermolecular interactions were calculated using a Lennard-Jones (LJ) potential and a Coulombic potential with fixed partial charges. All nonbonded interaction parameters were taken from the transferable potentials for phase equilibria (TraPPE) force field[39] that yields very satisfactory results for the phase behavior of neat CO_2,[39,40] binary mixtures with either alkanes[39] or methanol,[41] the negative partial molar volume of a naphthalene solute in $scCO_2$ near the critical point,[42] and the pressure and entrainer effects on its solubility characteristics.[43]

Simulations were performed for rigid linear CO_2 molecules ($\theta = 180°$) as well as rigid bent CO_2 molecules, for which the value of θ was taken to be 174.2°, which is the same as used in the modified EPM model by Zhang et al.[13] In addition, simulations were performed for a semirigid CO_2 molecule, where bond distances were fixed and the bend angle, θ, was allowed to fluctuate. For bent and semirigid CO_2, all LJ and Coulombic parameters were the same as for the linear TraPPE model.[39] For semirigid CO_2, a harmonic bend potential was fit to the potential energy surface of Chedin[24] (the same Chedin potential that was used without the harmonic approximation for the PIMC calculations) with a fixed bond length of 1.16 Å. The force constant and equilibrium bond angle were $k_\theta/k_B = 56920$ K/rad^2 and $\theta_e = 180°$. This force constant is significantly smaller than the value of $k_\theta/k_B = 148660$ K/rad^2 used for the flexible EPM2-M model proposed by Zhang et al.[13]

The semirigid TraPPE model was employed for canonical-ensemble Monte Carlo[44] simulations of the supercritical phase ($N = 350$ at $T = 325$ and 673 K and densities corresponding to a pressure of 10 MPa as provided by the Span and Wagner equation of state (EOS)).[45] Translational, rotational, and configurational-bias[46−48] Monte Carlo moves were used to sample phase space. A spherical cutoff at half the box length was used for LJ interactions with an analytic tail correction applied.[49] Ewald summation was used for the Coulombic interactions.[50] At least 1×10^5 MC cycles (where one MC cycle consists of 350 MC moves) of equilibration were performed, followed by 4×10^5 MC cycles of production. The resulting data were split into four equal-sized blocks for analysis.

Additional canonical-ensemble Monte Carlo simulations were carried out to compute the excess part of the constant-volume heat capacity of rigid linear, rigid bent, and semirigid CO_2 over a wider range of state points. For each model, twelve state points were simulated, corresponding to three temperatures ($T = 350$, 700, 1100 K) at four pressures ($p = 0.1$, 7.5, 10, 100 MPa). The density of each system and the reference value of the constant-volume heat capacity were taken from the EOS of Span and Wagner.[45]

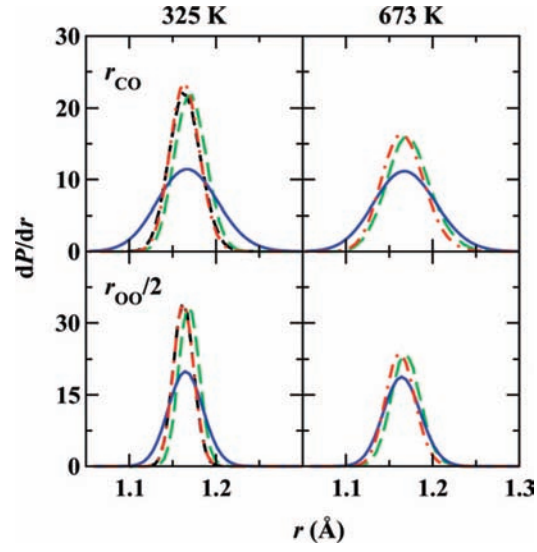

Figure 1. Internuclear distance distributions for the CO_2 molecule at 325 (left) and 673 K (right). The distributions obtained from PIMC calculations of an isolated molecule with $P = 256$ (325 K) or 128 (673 K) and $P = 1$ are shown as blue solid and red dot-dashed lines, respectively, and those obtained from FPMD simulations of the solid and high-density supercritical fluid phase are shown as black short-dashed and green long-dashed lines, respectively. A bin width of 0.005 Å is used.

3. Results and Discussion

The distributions of the internuclear distances (r_{CO} and $r_{OO'}$) and of their ratio ($f = r_{OO'}/(r_{CO} + r_{CO'})$) obtained from FPMD simulations of the solid and high-density supercritical phase and from PIMC calculations of an isolated molecule are compared in Figures 1 and 2, and the corresponding average values and root-mean-square deviations are listed in Table 1. Except for a small shift to larger internuclear distances by about 0.01 Å (which is primarily due to the difference in equilibrium C−O bond distance for an isolated molecule, namely a value of 1.173 Å for the BLYP functional and a value of 1.160 Å for the analytical potential used in the PIMC calculations), the data for the FPMD simulations and the PIMC calculations in the classical limit ($P = 1$) agree remarkably well for a given temperature. That is, neither the aggregation state (solid, supercritical fluid, and gas phase) nor the density of the supercritical fluid phase

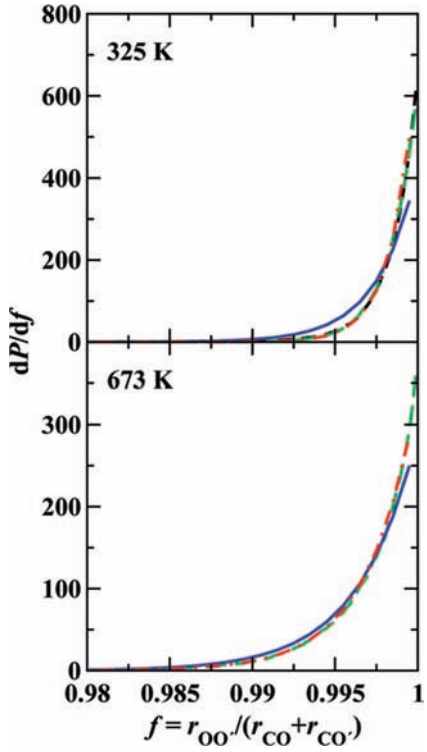

Figure 2. Distributions of the internuclear distance ratio, $r_{OO'}/(r_{CO} + r_{CO})$, at 325 (top) and 673 K (bottom). Colors as in Figure 1. A bin width of 0.001 is used.

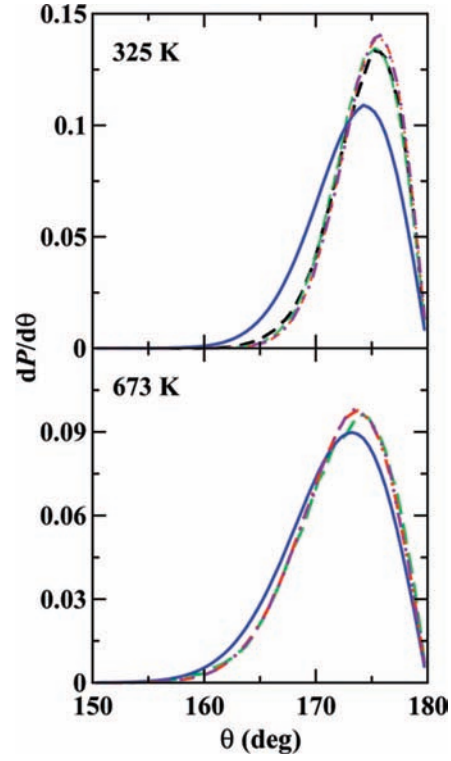

Figure 3. OCO′ angle distributions at 325 (top) and 673 K (bottom). The distributions obtained from Monte Carlo simulations of the supercritical phase using a semirigid TraPPE model are shown as violet dot-dot-dashed lines. Other colors as in Figure 1. A bin width of 0.5° is used.

appears to have a substantial influence on the internuclear distances. In contrast, either an increase in temperature from 325 to 673 K or the inclusion of nuclear quantum effects results in a significant broadening of the distribution of internuclear distances. As should be expected from the zero-point effect, the temperature dependence is less pronounced in the quantum mechanical limit.

All distributions for the internuclear distance ratio increase monotonically and exhibit a maximum for a ratio of unity (see Figure 2). This is in agreement with the data from neutron diffraction experiments.[17,18] However, since f can by definition not exceed a value of unity, the distributions are asymmetric and we obtain an average value of 0.9985 and a root-mean-square deviation from the mean of 0.0015 for the calculations that treat the nuclear motion in a fluid phase at 325 K classically including Monte Carlo simulations for the semirigid TraPPE model. The average value of 0.9984 for the FPMD simulation of the solid phase is slightly smaller, but this shift is within the uncertainties of the simulations. The f ratios obtained at 673 K and in the quantum mechanical limit are shifted to slightly smaller values and the root-mean-square deviations exhibit a significant increase compared to those obtained from classical sampling at 325 K.

The distributions of the bending angle are depicted as functions of θ and of cos θ in Figures 3 and 4. Again, it is immediately evident that the distributions obtained from FPMD simulations of the solid and supercritical phase, from MC simulations for the semirigid TraPPE model in the supercritical phase, and from PIMC calculations for an isolated molecule in the classical limit are in extremely good agreement, while those obtained in the quantum mechanical limit are broader. The peak in the linear distributions of θ is located at 175.7° for all classical mechanical calculations at 325 K, while the value in the quantum mechanical limit is shifted down to 174.3°. The good agreement of the peak position of 174.2° for the 32-molecule system

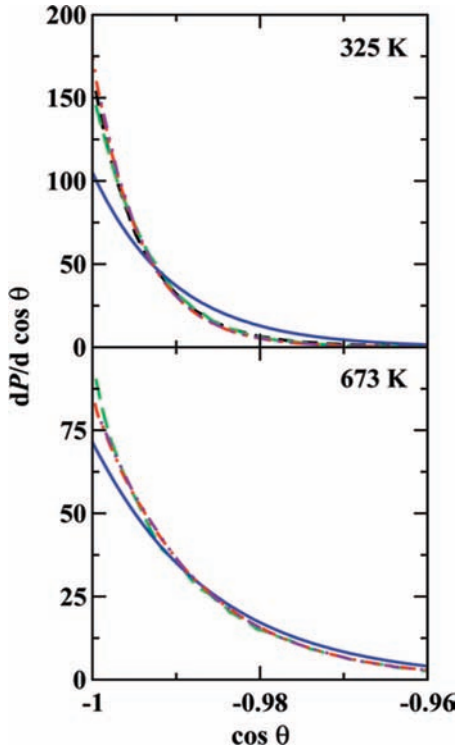

Figure 4. OCO′ angle distributions as a function of cos θ at 325 (top) and 673 K (bottom). Colors as in Figure 3.

average reported from CPMD simulations by Saharay and Balasubramanian[11] with the quantum mechanical value is entirely fortuitous as should be obvious from the very different widths of the distributions (with the distribution reported by

Saharay and Balasubramanian showing a negligible probability for $\theta > 175.5°$).

The asymmetry of the θ distributions obtained here (with an extended tail toward smaller θ values) results in average bending angles that are shifted down by about one degree compared to the peak positions (see Table 1). An increase of the temperature to 673 K again leads to broader distributions and consequently the peak positions and average bend angles are shifted to somewhat smaller values.

While the linear distributions of θ show a maximum for $\theta \neq 180$, the cosine distributions (see Figure 4) always show a maximum for a value of -1, i.e., a linear conformation. This difference is caused by the Jacobian factor, i.e., the nonuniform angular distribution of two randomly oriented unit vectors with the same origin that favors an angle of 90° and exhibits a vanishing probability for an angle of 180°. Thus, the cosine distributions indicate that CO_2 most favors a linear conformation compared to the random distribution of unit vectors, a result that should be obvious from its intramolecular potential energy surface that yields the linear structure as its global energy minimum.

It is very important to stress that our simulations do not indicate a significant difference in the cosine distributions obtained from FPMD simulations for the solid and (low- and high-density) supercritical phases and for the PIMC calculations with $P = 1$ for the isolated molecule. Hence, the dependence of the distributions on the aggregate state appears to be negligible. Saharay and Balasubramanian[12] found somewhat larger differences for CPMD simulations of $scCO_2$ at different densities. In particular, these authors emphasize the "contrasting behavior between the classical and CPMD simulations" (it should be noted here that both of these simulations follow classical mechanical trajectories that do not account for nuclear quantum effects). In contrast, our simulations show extremely good agreement for the distributions obtained from FPMD simulations and MC simulations for a semirigid empirical model with harmonic bond bending potential. As mentioned above, Saharay and Balasubramanian used the EPM2-M model developed by Zhang et al.[13] with a harmonic force constant that is about 2.6 times larger than the value used here, but with an equilibrium bond angle of 180° instead of $\theta_e = 174.2°$ used in the original EPM2-M model. Given the outstanding agreement between our MC simulations for the semirigid model and the FPMD and PIMC ($P = 1$) calculations, one must conclude that the force constant proposed by Zhang et al. is in error. Unfortunately, these authors do not indicate how the force constant was obtained, whereas our force constant is based on the accurate potential surface of Chedin.[24]

The θ and cos θ distributions obtained for the quantum mechanical limit differ significantly from those without nuclear quantum effects, but the difference is more pronounced at 325 K than at 673 K. Thus, any attempt to fit a harmonic force constant that reproduces the quantum mechanical distribution of bending angles would require a temperature-dependent force constant (e.g., values of 34 000 and 24 000 K/rad^2 at 325 and 673 K, respectively). The fact that Zhang et al.[13] obtained better predictions of the dielectric constant for a semirigid model as compared to a rigid model (with an equilibrium angle of 174.2° used in both cases) may be due to the Jacobian factor shifting downward the average bond angle of the semirigid model closer to the average value of 173.0° obtained here from PI calculations in the quantum mechanical limit at 325 K.

Due to the asymmetry of the angular and f distributions, not only the width of the distribution but also the peak position

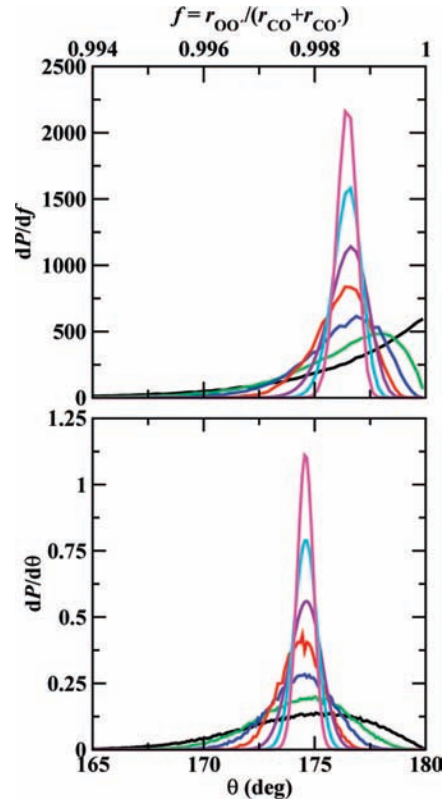

Figure 5. Dependence of internuclear distance ratio (top) and the OCO′ angle (bottom) distributions at 325 K on the group size, M, used for the observation. The distributions obtained from FPMD simulations of high-density $scCO_2$ for $M = 1$, 2, 4, and 8, and those obtained from PI calculations of an isolated molecule ($P = 1$) with $M = 16$, 32, and 64 are shown as black, green, blue, red, violet, cyan, and magenta lines, respectively. Bin widths of 0.0001 and 0.1 are used for the internuclear distance ratio and angle distribution plots, respectively.

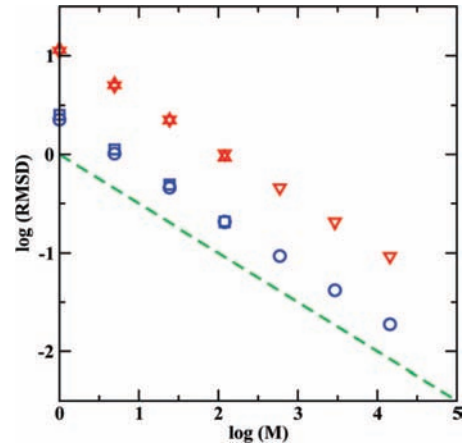

Figure 6. Logarithm of the root-mean-square deviations from the mean for the internuclear distance ratio (multiplied by 1000, blue symbols) and the OCO′ angle (red symbols) at 325 K as a function of the logarithm of the group size, M, used for the observation. Down triangles/circles and up triangles/squares correspond to data from PIMC calculations of an isolated molecule ($P = 1$) and from FPMD simulations for high-density $scCO_2$, respectively. The dashed green line indicates a slope of $-1/2$.

(but, of course, not the average value) will depend on the group size, M, for which an instantaneous average value is measured. This is illustrated in Figures 5 and 6. The distributions for cos θ and f obtained by considering each molecule separately (see Figures 2 and 4) exhibit their peak for the smallest/largest permissible value (cos $\theta = -1$ and $f = 1$). Hence, when

distributions are computed for data reflecting the instantaneous average value for M molecules, then the peak position shifts away from the smallest/largest permissible value and the distribution becomes more symmetric. This would ultimately lead to a delta function located at the average value. For example, the peak of the f distributions shifts from a value of $+1$ for $M = 1$ to 0.9988 for $M = 8$ and is close to the average value of 0.9986 for $M = 64$. The relative shift in the peak position for the θ distribution is less pronounced because the $M = 1$ distribution already peaks for $\theta < 180°$ due to the Jacobian factor.

The dependence of the root-mean-square deviations on M for the θ and f distributions is depicted in Figure 6. The rmsd values found for the PIMC ($P = 1$) and FPMD calculations are in excellent agreement. In all cases, the double logarithmic plot shows linear behavior with a slope close to $-1/2$, i.e., the value expected for a normal distribution of measurements.[51] Thus, a hypothetical experiment that instantaneously observes the average over a group of $M = 32$ molecules will lead to θ and f distributions with different widths and different peak positions than those obtained from a single-molecule experiment.

A very informative approach to elucidate whether a polyatomic molecule is effectively linear or nonlinear is the measurement/calculation of the heat capacity over a wide range of temperatures because the high-temperature limit of the heat capacity is $0.5R$ for a rotational degree of freedom (including only a kinetic energy term) whereas that for a harmonic vibrational degree of freedom is R (including both kinetic and potential energy contributions).[21] The common approach to compute the constant-volume heat capacity from a simulation that follows a classical mechanical trajectory is to determine only the excess part of the heat capacity (arising from intermolecular interactions) from a simulation in the canonical ensemble and to add analytical terms for the ideal gas part of the heat capacity (including the translational kinetic energy contribution for MC simulations).[50] The former part is usually evaluated from the fluctuations in the intermolecular energy[21] (if the energy can be cleanly separated such as for pairwise additive potentials, but care is required for polarizable force fields[52,53] or first principles simulations[54]) and the intramolecular part of the latter is often estimated using the rigid rotor/harmonic oscillator (RR/HO) approximation.[21]

In this work, we assume that the classical limit can be applied for the rotational degrees of freedom and, hence, each of these degrees of freedom contributes $0.5R$ to the heat capacity. On the other hand, the quantum mechanical formula is used for the vibrational degrees of freedom.[21] This formula requires knowledge of the vibrational frequencies of an isolated CO_2 molecule. Here, we use two different sets of frequencies: (i) 673, 1354, and 2396 cm^{-1}, the harmonic frequencies determined from a fit to the curvature at the global energy minimum on the potential energy surface of Chedin,[24] and (ii) 667, 1388, and 2349 cm^{-1}, the fundamental frequencies obtained from the experimentally observed overtones.[55] To some extent, the fundamental frequencies account for the anharmonicity of the true vibrations and, hence, may lead to improved accuracy compared to harmonic frequencies when used in the HO formulas.[56] Given that the linear conformer is the minimum energy structure, it is not trivial to evaluate the harmonic frequencies for a bent structure and we assume that the frequencies remain the same but that one of the two degenerate bending modes is replaced by a rotational mode when calculating the RR/HO heat capacities for the bent structure.

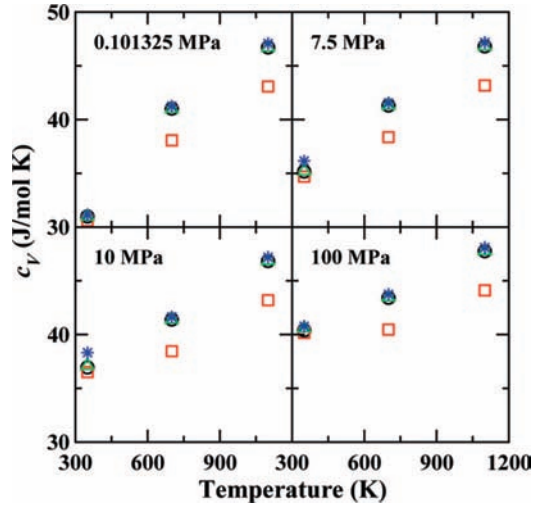

Figure 7. Constant-volume heat capacity of CO_2 as a function of temperature at four different densities corresponding to the pressures listed in the figure. The values obtained from an EOS[45] fitted to a large experimental data set are shown as blue stars. Black circles, red squares, and green triangles depict data obtained from Monte Carlo simulations for a rigid linear model, a rigid nonlinear model ($\theta = 174.2°$), and a semirigid model ($\theta_{eq} = 180.0°$), respectively, in conjunction with the rigid rotor/harmonic oscillator approximation (using the harmonic frequencies) to account for the contribution of vibrational and rotational degrees of freedom.

Figure 7 shows a comparison of the constant-volume heat capacities of CO_2 obtained for different empirical models over a wide range of temperatures ($>T_{crit}$) and densities. The different models are validated against pseudoexperimental values obtained from a very accurate EOS.[45] The data show that both the rigid linear and the semirigid models yield C_V values that agree well with the EOS, whereas use of the rigid bent model leads to C_V values that are only satisfactory at 350 K, but are significantly too small at 700 and 1100 K. This comparison unequivocally demonstrates that CO_2 should not be viewed as a nonlinear molecule and, hence, should not be described by a nonlinear model. However, it can of course be represented by a flexible model that has an equilibrium angle of 180°. Here it should also be noted that the C_V values calculated for the TraPPE force field are in excellent agreement with the experimental data with the exception of the two state points closest to the critical point ($T = 350$ K and $p = 7.5$ or 10 MPa) where C_V is slightly underestimated. The excess C_V computed for the rigid and semirigid TraPPE models are very close for all state points, i.e., the differences in the energetics of the neat $scCO_2$ phase are very small.

The numerical values of the rovibrational heat capacity contribution, C^{rovib}, obtained from PIMC calculations and various approximations are summarized in Table 2. The PIMC calculations with $P = 1$ yield C^{rovib} values close to 5 R, the classical limit for a linear triatomic molecule, at all temperatures. At 325 K, the RR/HO values for both linear and bent CO_2 molecules agree well with the PIMC calculations for the quantum mechanical limit. The relatively small differences for the RR/HO values for linear and bent CO_2 at 325 K are due to a fortuitous cancelation, i.e., the HO value for C^{vib} for the bending mode is close to $0.5R$ at room temperature.[21] However, the C^{rovib} values at 673 and 1100 K show that only the RR/HO values for the linear structure agree with the EOS values and PIMC calculations for the quantum mechanical limit and, hence, demonstrate that CO_2 must be viewed as a linear molecule.

Finally, a comparison to the C^{rovib} values obtained from the EOS demonstrates the accuracy of the PIMC calculations in

the quantum mechanical limit (and, hence, of the underlying potential energy surface) that gives a mean percentage deviation of only 0.2%. In contrast, the RR/HO approximation of the linear molecule yields mean percentage deviations of 1.9% and 0.9% for the fundamental and harmonic frequencies, respectively.

4. Conclusions

PIMC calculations for an isolated molecule, FPMD simulations for the solid and supercritical phase, and MC simulations for the semirigid TraPPE model in the supercritical phase allow the following conclusions. First, CO_2 most favors an arrangement with the second CO bond being collinear with respect to the first, but the Jacobian factor leads to a peak in the angular distribution at 175.7° and a mean bend angle of 174.5° in the classical limit at $T = 325$ K. Second, the dependence of the distributions of the internuclear distance ratio, the bend angle, and the cosine of the bend angle on the aggregation state (solid, supercritical, or ideal gas phase) is negligible, whereas changes in temperature or inclusion of nuclear quantum effects significantly alter these distributions. Third, when one considers angular and distance ratio distributions of mean values in groups (rather than distributions of individual values), the peak values and the widths of the distributions depend on the group size. Fourth, the heat capacity is accurately reproduced only by models that use a linear equilibrium structure.

Acknowledgment. We thank Fabrizio Lo Celso and Francesco Ferrante for stimulating discussions. Financial support from the National Science Foundation (ITR-0428774, CBET-0756641, and CHE-0704974) and a Doctoral Dissertation Fellowship (K.E.A.) is gratefully acknowledged. Part of the computer resources were provided by the Minnesota Supercomputing Institute.

References and Notes

(1) Hannay, J. B.; Hogarth, J. *Proc. Roy. Soc. London* **1879**, *29*, 324.
(2) McHugh, M. A.; Krukonis, V. J. *Supercritical Fluid Extraction: Principles and Practice,* 2nd ed.; Butterworth: Boston, MA, 1994.
(3) Dobbs, J. M.; Wong, J. M.; Johnston, K. P. *J. Chem. Eng. Data* **1986**, *31*, 303.
(4) Dobbs, J. M.; Wong, J. M.; Lahiere, R. J.; Johnston, K. P. *Ind. Eng. Chem. Res.* **1987**, *26*, 56.
(5) Eckert, C. A.; Ziger, D. H.; Johnston, K. P.; Kim, S. *J. Phys. Chem.* **1986**, *90*, 2738.
(6) Brennecke, J. F.; Eckert, C. A. *AIChE J.* **1989**, *35*, 1409.
(7) Eckert, C. A.; Knutson, B. L.; Debenedetti, P. G. *Nature* **1996**, *383*, 313.
(8) Tucker, S. C. *Chem. Rev.* **1999**, *99*, 391.
(9) Martin, M. G.; Chen, B.; Siepmann, J. I. *J. Phys. Chem. B* **2000**, *104*, 2415.
(10) Saharay, M.; Balasubramanian, S. *J. Chem. Phys.* **2004**, *120*, 9694.
(11) Saharay, M.; Balasubramanian, S. *ChemPhysChem* **2004**, *5*, 1442; Erratum *ChemPhysChem* **2006**, *7,* 1167.
(12) Saharay, M.; Balasubramanian, S. *J. Phys. Chem. B* **2007**, *111*, 387.
(13) Zhang, Y.; Yang, J.; Yu, Y.-X. *J. Phys. Chem. B* **2005**, *109*, 13375.
(14) Harris, J. G.; Yung, K. H. *J. Phys. Chem.* **1995**, *99*, 12021.
(15) Lo Celso, F.; Triolo, R.; Ferrante, F.; Botti, A.; Bruni, F.; Mancinelli, R.; Ricci, M. A.; Soper, A. K. *J. Mol. Liq.* **2007**, *136*, 294.
(16) Botti, A.; Bruni, F.; Mancinelli, R.; Ricci, M. A.; Lo Celso, F.; Triolo, R.; Ferrante, F.; Soper, A. K. *J. Chem. Phys.* **2008**, *128*, 164504.
(17) Adya, A. K.; Wormald, C. J. *Mol. Phys.* **1991**, *74*, 735.
(18) Ishii, R.; Okazaki, S.; Odawara, O.; Okada, I.; Misawa, M.; Fukunaga, T. *Fluid Phase Equilib.* **1995**, *104*, 291.
(19) Karle, I. L.; Karle, J. *J. Chem. Phys.* **1949**, *17*, 1052.
(20) van Tricht, J. B.; Fredrikze, H.; van der Laan, J. *Mol. Phys.* **1984**, *52*, 115.
(21) McQuarrie, D. A. *Statistical Mechanics*; University Science Books: Sausalito, CA, 2000.
(22) Feynman, R. P. *Statistical Mechanics*; Benjamin: Reading, PA, 1972.
(23) Feynman, R. P.; Hibbs, A. R. *Quantum Mechanics and Path Integrals*; McGraw-Hill: New York, NY, 1965.
(24) Chedin, A. *J. Mol. Spectrosc.* **1979**, *76*, 430.
(25) Lynch, V. A.; Mielke, S. L.; Truhlar, D. G. *J. Chem. Phys.* **2004**, *121*, 5148.
(26) Mielke, S. L.; Srinivasan, J.; Truhlar, D. G. *J. Chem. Phys.* **2000**, *112*, 8758.
(27) Mielke, S. L.; Truhlar, D. G. *J. Chem. Phys.* **2001**, *114*, 621.
(28) Mielke, S. L.; Truhlar, D. G. *Chem. Phys. Lett.* **2003**, *378*, 317.
(29) Predescu, C.; Sabo, D.; Doll, J. D.; Freeman, D. L. *J. Chem. Phys.* **2003**, *119*, 12119.
(30) Yamamoto, T. M. *J. Chem. Phys.* **2005**, *123*, 104101.
(31) VandeVondele, J.; Krack, M.; Mohamed, F.; Parrinello, M.; Chassaing, T.; Hutter, J. *Comput. Phys. Commun.* **2005**, *167*, 103.
(32) Lippert, G.; Hutter, J.; Parrinello, M. *Mol. Phys.* **1997**, *92*, 477.
(33) Kohn, W.; Sham, L. J. *Phys. Rev. A* **1965**, *140*, 1133.
(34) Becke, A. D. *Phys. Rev. A* **1988**, *38*, 3098.
(35) Lee, C.; Yang, W.; Parr, R. G. *Phys. Rev. B* **1988**, *37*, 785.
(36) VandeVondele, J.; Hutter, J. *J. Chem. Phys.* **2007**, *127*, 114105.
(37) Goedecker, S.; Teter, M.; Hutter, J. *Phys. Rev. B* **1996**, *54*, 1703.
(38) Martyna, G. J.; Klein, M. L.; Tuckerman, M. E. *J. Chem. Phys.* **1992**, *97*, 2635.
(39) Potoff, J. J.; Siepmann, J. I. *AIChE J.* **2001**, *47*, 1676.
(40) Chen, B.; Siepmann, J. I.; Klein, M. L. *J. Phys. Chem. B* **2001**, *105*, 9840.
(41) Stubbs, J. M.; Siepmann, J. I. *J. Chem. Phys.* **2004**, *121*, 1525.
(42) Stubbs, J. M.; Drake-Wilhelm, D. D.; Siepmann, J. I. *J. Phys. Chem. B* **2005**, *109*, 19885.
(43) Anderson, K. E.; Siepmann, J. I. *J. Phys. Chem. B* **2008**, *112*, 11374.
(44) Metropolis, N.; Rosenbluth, A. W.; Rosenbluth, M. N.; Teller, A. H.; Teller, E. *J. Chem. Phys.* **1953**, *21*, 1087.
(45) Span, R.; Wagner, W. *J. Phys. Chem. Ref. Data* **1996**, *25*, 1509.
(46) Siepmann, J. I.; Frenkel, D. *Mol. Phys.* **1992**, *75*, 59.
(47) Vlugt, T. J. H.; Martin, M. G.; Smit, B.; Siepmann, J. I.; Krishna, R. *Mol. Phys.* **1998**, *94*, 727.
(48) Martin, M. G.; Siepmann, J. I. *J. Phys. Chem. B* **1999**, *103*, 4508.
(49) Wood, W. W.; Parker, F. R. *J. Chem. Phys.* **1957**, *27*, 720.
(50) Allen, M. P.; Tildesley, D. J. *Computer Simulation of Liquids*; Oxford University Press: Oxford, UK, 1987.
(51) Taylor, J. R. *An Introduction to Error Analysis: The Study of Uncertainties in Physical Measurements*; University Science Books: Sausalito, CA, 1997.
(52) Chen, B.; Siepmann, J. I. *Theor. Chem. Acc.* **1999**, *103*, 87.
(53) Chen, B.; Potoff, J. J.; Siepmann, J. I. *J. Phys. Chem. B* **2000**, *104*, 2378.
(54) Kuo, I.-F. W.; Mundy, C. J.; McGrath, M. J.; Siepmann, J. I.; VandeVondele, J.; Sprik, M.; Hutter, J.; Chen, B.; Klein, M. L.; Mohamed, F.; Krack, M.; Parrinello, M. *J. Phys. Chem. B* **2004**, *108*, 12990.
(55) Suzuki, I. *J. Mol. Spectrosc.* **1968**, *25*, 479.
(56) Truhlar, D. G.; Isaacson, A. D. *J. Chem. Phys.* **1991**, *94*, 357.

JP808711Y